

# HOMOGENIZATION OF THE PHYSICALLY NONLINEAR PROPERTIES OF THREE-DIMENSIONAL METAL MATRIX COMPOSITES USING THE NONUNIFORM TRANSFORMATION FIELD ANALYSIS

F. Fritzen<sup>†</sup> and T. Böhlke

Chair of Continuum Mechanics, Institute of Engineering Mechanics,  
University of Karlsruhe (TH), Post Box 6980, 76128 Karlsruhe, Germany  
(<sup>†</sup>*corresponding author*: fritzen@itm.uni-karlsruhe.de)

## SUMMARY

The inelastic material properties of Metal Matrix Composites with particulate reinforcement are investigated. A method for the generation and spatial discretization of a class of model microstructures is presented. The Nonuniform Transformation Field Analysis is employed to examine the microheterogeneous material. Numerical examples are presented.

*KEYWORDS: homogenization, mesh generation, metal matrix composites (MMC), nonuniform transformation field analysis (NTFA)*

## 1. INTRODUCTION

The development of microheterogeneous materials has been enforced in the past two decades with the main aim being an improvement in the weight-strength ratio of engineering structures. Additionally, multiphysics applications have seen increasing attention lately. An example for the latter is thermal management where the mechanical and the thermal properties of the material are optimized in a coupled procedure.

The linear thermal and mechanical properties of microheterogeneous materials are well understood for many materials and a variety of homogenization methods has been proposed in the past century (see e.g. [1] for a summary). Prominent analytical and semi-analytical methods for the homogenization are the upper Voigt bound and the lower Reuss bound, the Hashin-Shtrikman variational principle [2], the Mori Tanaka method [3] and the self-consistent scheme by Kröner [4]. Numerical computations have shown that these methods can determine the linear properties of many microheterogeneous materials to a sufficient extent (e.g. [5]) if the contrast in the physical properties (thermal conductivity; elastic moduli) is small enough.

When non-linear material properties are observed many of the assumptions entering the mentioned methods are no longer satisfied. Particularly, the stress and strain fields become nonlinear functions when inelastic deformations are accounted for on the microscopic level. This evolution cannot be determined (semi-) analytically due to severe path dependency. To overcome these short-comings, several numerical methods have been developed. A numerical multiscale method is the multi-level Finite Element Method (FE<sup>p</sup>). The method has seen massive attention for two-dimensional problems (e.g. [6]). Fur-

ther, the technique has been extended to generalized continua in [7]. The large degree of freedom with respect to the modelling of materials and structures when using a multi-level FE approach in return leads to excessive number of degrees of freedom even for two-dimensional problems. Application to three-dimensional problems is still limited, despite the ever increasing amount of available memory and cpu power. It has to be mentioned that, usually,  $FE^p$  requires massive parallelization which precludes application of the method for a broader audience.

A method for the condensation of the number of degrees of freedom was proposed by Dvorak [8, 9] in terms of the Transformation Field Analysis (TFA). In the latter the plastic strain fields are assumed to be constant in subdomains of the microscopic material. Hence, only few coefficients need to be computed. The method has been applied for the homogenization of non-linear material properties of materials at acceptable numerical cost. However, the method has shown to provide rather stiff response [10].

To overcome this overly stiff prediction of the effective material response of the unit cell it has been proposed by Michel, Suquet and co-workers [11, 12, 13] to extend the TFA to the case where the plastic strain fields are no longer constant. More precisely, the characteristic deformation patterns of composite structures can be replicated using only few scalar coefficients. The method has been applied to two-dimensional composites with great success [11, 12, 13].

In this paper we apply the NTFA to random three-dimensional model microstructures resembling particulate MMCs in the absence of damage, i.e. linear elastic particles and a ductile matrix material are considered. The latter are based on the Voronoi tessellation of a random set of points. Section 2 is devoted to the generation of the geometry and the spatial discretization of the latter. In Section 3 we briefly revisit the constitutive equations of the NTFA and derive equations describing the macroscopic material behaviour using the internal variable. The effective stress strain response of the homogenized material is compared to the one of full-field unit cell computations in Section 4.

## 2. MODEL MICROSTRUCTURES

Model microstructures based on Voronoi tessellations have been used for polycrystalline aggregates in the past ([14] and others). The authors have recently proposed a fast mesh generator based on the Voronoi tessellation which creates not only periodic microstructures but also periodic mesh topologies while the geometry is exactly replicated [5]. In this section we describe a modification of the procedure described in [5] for the construction of three-dimensional model microstructures consisting of a matrix material and polygonal particulate inclusions.

First, a (for simplicity) cuboidal unit cell of the type

$$\Omega = [-w/2, w/2] \times [-d/2, d/2] \times [-h/2, h/2] \subset \mathbb{R}^3 \quad (1)$$

is considered. Then a set of  $N$  random points  $P_i \in \Omega$  is generated and copied 26 times around to unit cell in order to define a periodic Voronoi tessellation [15]. A point  $X \in \Omega$  is part of the Voronoi cell defined by the point  $P_i$  which has the smallest (Euclidean)

distance to  $X$ . The cells of a Voronoi tessellation are convex bounded polyhedra which can either be characterized by their corner vertices or in terms of the intersection of a set of  $m$  halfspaces, with  $m$  being the number of faces of the cell. The two representations are dual to each other.

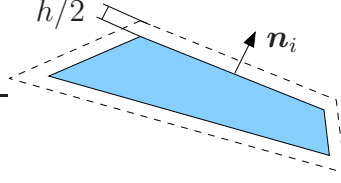


Figure 1: Shrinking a convex polyhedron (here: in 2d)

Each of the halfspaces  $H_i$  can be characterized by its outward unit normal vector  $\mathbf{n}_i$  and the offset  $\delta_i$  from the origin. Suppose now that a cell is defined by a set of  $M$  tuples  $\{\mathbf{n}_i, \delta_i\}_{i=1, \dots, M}$ . By modifying the offset parameter via

$$\delta_i^* = \delta_i - \frac{h}{2}, \quad (2)$$

all cell faces are translated in negative unit normal direction forming a separating layer of thickness  $h$  between neighboring cells (Fig. 1). The cells constructed using this method have the following properties:

- Cells can vanish during the shrinking process due to their small initial size.
- The remaining cells are convex.
- All cells have a uniform distance to their direct neighbors, i.e. there is no penetration and no percolation.
- The number of faces of the new cell is smaller or equal the number of faces on the original cell.
- The volume fraction of the cells (representing the inclusions) can easily be scaled by modification of the parameter  $h$ .
- The microstructure is periodic. This allows to endow the unit cell with periodic displacement boundary conditions or anti-periodic traction boundary conditions (e.g. [6] and others).

With the definition of the faces of the inclusions a periodic three-dimensional mesh can be obtained by the procedure described in [5] with minor modifications. Particularly, the filler material has to be added to the mesh and the surface mesh on the faces of the unit cell has to be modelled with care. It is noteworthy that the advantages of the mesh generation algorithm such as fast mesh generation and fully scalable mesh density apply to this new class of model microstructures. Additionally, it is possible to modify the point seed  $P_i$  by superimposing a hardcore condition etc.

Example meshes for  $N = 5$  and 200 are shown in Fig. 2. Remarkably, the larger the number of inclusions the denser the mesh has to be in order to expect proper results from

a finite element analysis. This may quickly lead to several million degrees of freedom in a purely mechanical analysis. Hence, such discrete microstructures are not recommended for application with  $FE^p$  methods [7, 16].

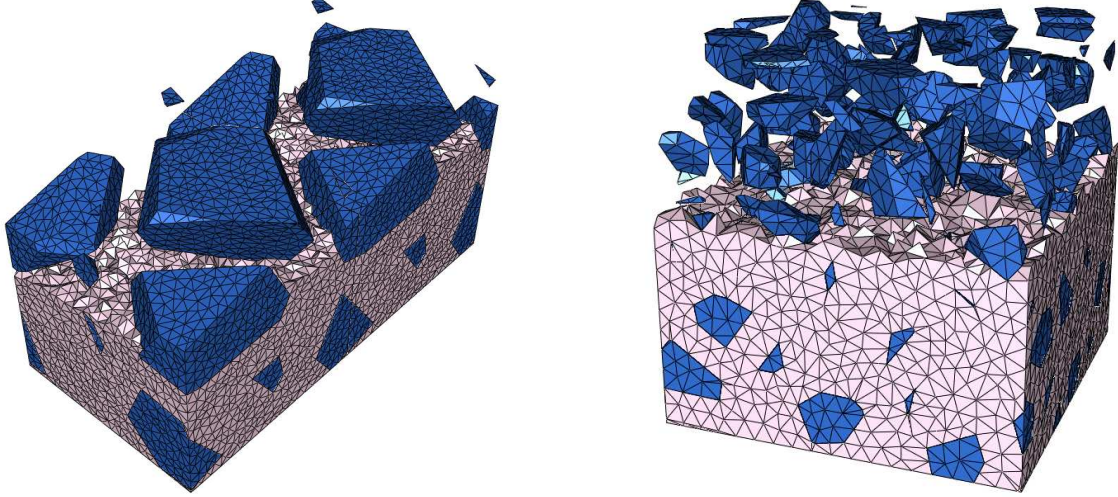


Figure 2: Example meshes for  $N = 5$  (left with periodic continuation), 200 (right)

### 3. NONUNIFORM TRANSFORMATION FIELDS

In the following we restrict ourselves to mechanical two-scale problems in a small deformation setting. The stress  $\sigma$ , strain  $\varepsilon$  and the displacement  $u$  are assumed on the microscopic scale (unit cell level), whereas overlined quantities are taken at the macroscopic (structural) level on the domain  $\bar{\Omega}$  with boundary  $\bar{\Gamma} = \partial\bar{\Omega}$ . The macroscopic and the microscopic fields are related by the averaging operator  $\langle \bullet \rangle$ :

$$\bar{\varepsilon} = \langle \varepsilon \rangle, \quad \bar{\sigma} = \langle \sigma \rangle. \quad (3)$$

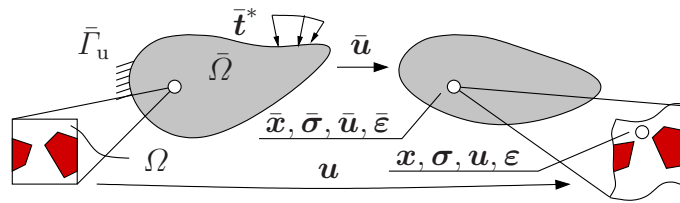


Figure 3: Macroscopic (structural) problem and associated microscopic problem

Then the homogenization problem persists in solving

$$(\bar{P}) : \begin{cases} \operatorname{div}(\bar{\sigma}) = \mathbf{0} & \text{in } \bar{\Omega}, \\ \bar{\sigma} \bar{n} = \bar{t} = \bar{t}^* & \text{on } \bar{\Gamma}_t \subsetneq \bar{\Gamma}, \\ \bar{u} = \bar{u}^* & \text{on } \emptyset \neq \bar{\Gamma}_u \subset \bar{\Gamma}, \end{cases} \quad \text{and } (P) : \begin{cases} \operatorname{div}(\sigma) = \mathbf{0} & \text{in } \Omega, \\ \langle \varepsilon \rangle = \bar{\varepsilon}, \\ \sigma & \text{admissible,} \end{cases} \quad (4)$$

where the admissible domain of  $\sigma$  is, e.g., defined by the yield surface of an elasto-plastic material.

The major assumption of the NTFA is the existence of a finite dimensional basis spanned by plastic strain fields  $\boldsymbol{\mu}^{(i)}(\mathbf{x})$  ( $i = 1, \dots, N < \infty$ ), such that the plastic strain field  $\boldsymbol{\varepsilon}^p$  can be approximated by  $\boldsymbol{\varepsilon}_{\text{app}}^p$  for some  $\delta_p > 0$ , such that

$$\boldsymbol{\varepsilon}_{\text{app}}^p(t, \mathbf{x}) = \sum_{i=1}^N \xi^{(i)}(t) \boldsymbol{\mu}^{(i)}(\mathbf{x}), \quad \|\boldsymbol{\varepsilon}_{\text{app}}^p(t, \mathbf{x}) - \boldsymbol{\varepsilon}^p(t, \mathbf{x})\| < \delta_p \quad (5)$$

for some suitable norm usually involving volume averaging over the unit cell (e.g. the  $L^2_\Omega$  norm). Obviously (5) cannot be satisfied for arbitrary deformation processes. However, it can be observed that real materials show characteristic deformation patterns, e.g. plastification in regions close to stiffer inclusions. These patterns are massively influenced by both, the physical properties of the material (anisotropy, nonlinearity) and the topology of the heterogeneous medium. The latter can for example be described by means of  $n$ -point correlation functions [17].

The idea of the NTFA persists in trying to determine (a small but sufficient number of) plastic modes  $\boldsymbol{\mu}^{(i)}$  associated with the characteristic deformations of a unit cell in a numerical testing environment and then to formulate appropriate evolution equations for the coefficients  $\xi^{(i)}(t)$ . The local stress and strain field at position  $\mathbf{x}$  and time  $t$  can be expressed in terms of  $\boldsymbol{\xi}(t)$  and the strain concentration tensor  $\mathbb{A}(\mathbf{x})$

$$\boldsymbol{\varepsilon}(\mathbf{x}, t) = \mathbb{A}(\mathbf{x})[\bar{\boldsymbol{\varepsilon}}] + \sum_{j=1}^N \xi^{(j)}(t) \boldsymbol{\varepsilon}_*^{(j)}(\mathbf{x}), \quad (6)$$

$$\boldsymbol{\sigma}(\mathbf{x}, t) = \mathbb{C}(\mathbf{x})\mathbb{A}(\mathbf{x})[\bar{\boldsymbol{\varepsilon}}] + \sum_{j=1}^N \xi^{(j)}(t) \boldsymbol{\sigma}_*^{(j)}(\mathbf{x}). \quad (7)$$

Following the method introduced in [11, 12] the thermodynamic driving forces are:

$$\tau^{(i)} = \langle \mathbb{A}^\top \mathbb{C}[\boldsymbol{\mu}^{(i)}] \rangle \cdot \bar{\boldsymbol{\varepsilon}} + \sum_{j=1}^N \xi^{(j)} \langle \boldsymbol{\mu}^{(i)} \cdot \boldsymbol{\sigma}_*^{(j)} \rangle = \langle \mathbb{A}^\top \mathbb{C}[\boldsymbol{\mu}^{(i)}] \rangle \cdot \bar{\boldsymbol{\varepsilon}} + \mathbf{D}\boldsymbol{\xi}, \quad (8)$$

with  $\boldsymbol{\sigma}_*^{(j)} = \mathbb{C}[\boldsymbol{\varepsilon}_*^{(j)} - \boldsymbol{\mu}^{(j)}]$  the solution of the eigenstress problem

$$(P_\sigma^j) : \quad \text{div}(\mathbb{C}[\boldsymbol{\varepsilon}_*^{(j)} - \boldsymbol{\mu}^{(j)}]) = \mathbf{0}, \quad \langle \boldsymbol{\varepsilon}_*^{(j)} \rangle = \mathbf{0}. \quad (9)$$

We assert that the modes satisfy the restrictions of [11, 12]:

- The modes are normalized ( $\langle \|\boldsymbol{\mu}^{(i)}\|_2 \rangle = 1$ ).
- The modes are linearly independent and the support of individual modes is restricted to one phase.
- The modes are orthogonal ( $\langle \boldsymbol{\mu}^{(i)} \cdot \boldsymbol{\mu}^{(j)} \rangle = 0$  ( $i \neq j$ )).

A suitable evolution equation for the internal variables  $\xi^{(i)}$  has been found to be

$$\dot{\xi}^{(i)} = \lambda \frac{\tau^{(i)}}{\|\boldsymbol{\tau}\|_2} \quad (10)$$

for a material showing plasticity of von Mises type. The variable  $\dot{\lambda}$  is a Lagrangian multiplier satisfying the Karush-Kuhn-Tucker complementary conditions

$$\dot{\lambda}\varphi = 0, \quad \dot{\lambda} \geq 0, \quad \text{for } \varphi(\boldsymbol{\tau}, \bar{q}) = \|\boldsymbol{\tau}\|_2 - \sqrt{2/3} \sigma_F(\bar{q}). \quad (11)$$

The variable  $\bar{q}$  is an additional internal variable accounting for isotropic hardening effects. The latter is assumed constant over the entire unit cell, i.e. it has a spatially uniform distribution. The evolution equation for the hardening variable is

$$\dot{\bar{q}} = \dot{\lambda} \sqrt{\frac{2}{3}}. \quad (12)$$

As an important outcome of (7), the macroscopic stress  $\bar{\boldsymbol{\sigma}}$  is a linear transformation of the macroscopic strain  $\bar{\boldsymbol{\varepsilon}}(t)$  and coefficients  $\boldsymbol{\xi}(t)$ :

$$\begin{aligned} \bar{\boldsymbol{\sigma}}(\bar{\boldsymbol{\varepsilon}}(t), \boldsymbol{\xi}(t)) &= \langle \mathbb{C}(\mathbf{x}) \mathbb{A}(\mathbf{x}) \rangle [\bar{\boldsymbol{\varepsilon}}] + \sum_{j=1}^N \xi^{(j)}(t) \langle \boldsymbol{\sigma}_*^{(j)} \rangle \\ &= \bar{\mathbb{C}}[\bar{\boldsymbol{\varepsilon}}] + \sum_{j=1}^N \xi^{(j)}(t) \langle \boldsymbol{\sigma}_*^{(j)} \rangle. \end{aligned} \quad (13)$$

## 4. NUMERICAL EXAMPLES

### 4.1 Problem setting

The NTFA is implemented into ABAQUS/STANDARD using an implicit time integration procedure based on the Backward Euler scheme to integrate (11) and (12) on the interval  $[t_n, t_{n+1}]$ .

In a first step we examine the efficiency of the NTFA at integration point level. More precisely, we define an arbitrary proportional strain path to (i) a full field unit cell computation and (ii) the homogenized material model. The following quantities are then compared: (i) the macroscopic stress  $\bar{\boldsymbol{\sigma}}$ , (ii) the average plastic strain  $\langle \boldsymbol{\varepsilon}_p \rangle$  in the metal phase and (iii) the component  $\sigma_{23}$  of the stress field (full field vs. reconstructed field). The strain rate of the process considered here is

$$\dot{\bar{\boldsymbol{\varepsilon}}} = \begin{pmatrix} -0.01027 & 0.07142 & 1.6983 \\ & 0.15701 & 1.8680 \\ \text{sym.} & & -0.1467 \end{pmatrix} \mathbf{e}_i \otimes \mathbf{e}_j \quad \text{s}^{-1}. \quad (14)$$

It is held constant during the process time  $T = 0.05\text{s}$ . A total of only six different modes has been chosen for the model microstructure containing three linear elastic particles ( $\approx 18.45\%$  vol. fraction). The material parameters for the inclusions are set to the ones of polycrystalline Alumina ( $\text{Al}_2\text{O}_3$ ,  $E = 375 \text{ GPa}$ ,  $\nu = 0.22$ ). The matrix material is aluminium (AlSi12) with nonlinear isotropic hardening of the type

$$\sigma_F(q) = \sigma_0 + hq + \Delta\sigma(1 - \exp(-kq)), \quad (15)$$

with  $q$  a strain like hardening variable ressembling the equivalent plastic strain and non-negative material parameters  $\sigma_0, \Delta\sigma, k$  ( $E = 70 \text{ GPa}$ ,  $\nu = 0.32$ ,  $\sigma_0 = 80 \text{ MPa}$ ,  $\Delta\sigma = 40$

MPa,  $h = 50$  MPa,  $k = 23.75$ ). The large degree of nonuniformity of the plastic strain field, the displacement field and the stress field is exemplified in Fig. 4 for the first inelastic mode (scales normalized) which has been identified from a numerical test at macroscopic strain rate

$$\dot{\bar{\epsilon}} = \dot{\epsilon}_0/2(2\mathbf{e}_1 \otimes \mathbf{e}_1 - \mathbf{e}_2 \otimes \mathbf{e}_2 - \mathbf{e}_3 \otimes \mathbf{e}_3). \quad (16)$$

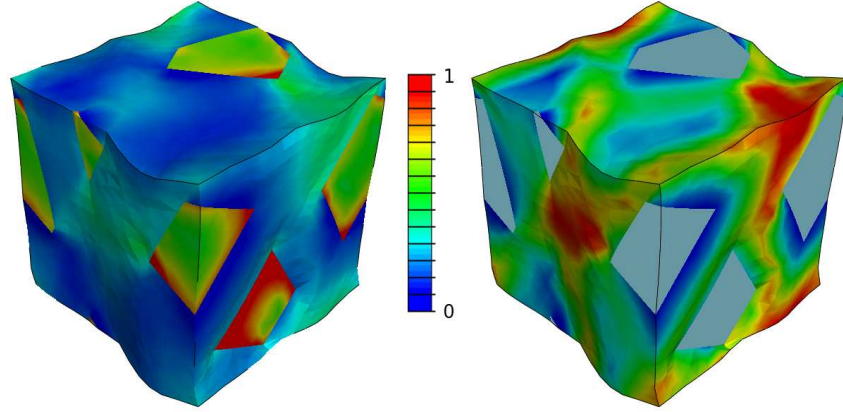


Figure 4: Plastic Mode 1: induced von Mises stress  $\sigma_{vM}$  (right);  $\epsilon_{11}^p$  (left)

#### 4.2 Time history of macroscopic average stresses and plastic strains

The time history of macroscopic stress tensor of the full field computation  $\bar{\sigma}^{\text{ref}}$  and the NTFA  $\bar{\sigma}^{\text{NTFA}}$  are compared in Fig. 5. The diagonal components (Fig. 5; left) and the shear components (Fig. 5; right) have been separated for clarity.

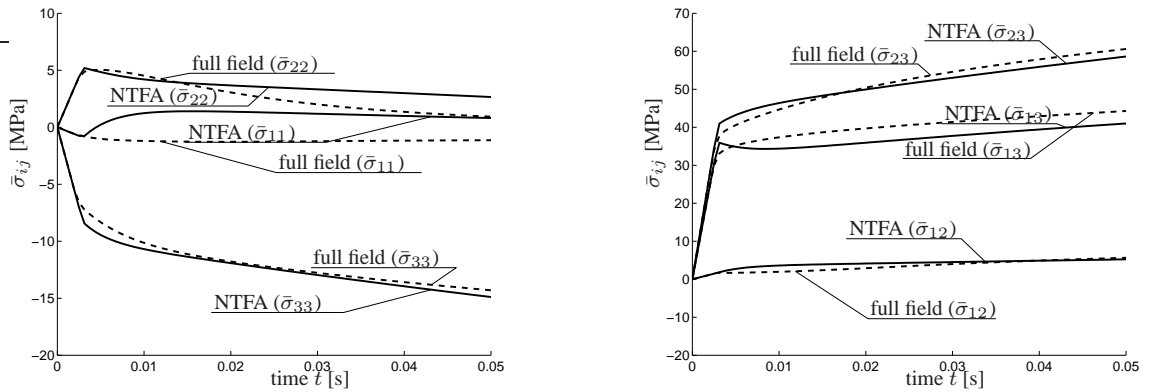


Figure 5: Time history of  $\bar{\sigma}_{11}$ ,  $\bar{\sigma}_{22}$ ,  $\bar{\sigma}_{33}$  (left) and  $\bar{\sigma}_{12}$ ,  $\bar{\sigma}_{13}$ ,  $\bar{\sigma}_{23}$  (right)

A good agreement was found for the components of the macroscopic stress with excellent results for the shear directions which are subjected to larger strains (see (14)). While the relative deviation of the normal components of  $\bar{\sigma}$  show some discrepancy between the NTFA and the reference computation it has to be pointed out that the relative error with respect to  $\|\bar{\sigma}\|$  are in the order of  $5 \cdot 10^{-3}$  and smaller.

Additionally, we have evaluated the components of the average of the plastic strain tensor, where the average has been taken with respect to  $\Omega_p$ , i.e. with respect to the inelastic volume. The results are shown in Fig. 6. Again, normal and shear components have been separated. Remarkably, there are almost no deviations between the full field simulation and the NTFA prediction. Hence, the requirement (5) holds for a small  $\delta_p$ .

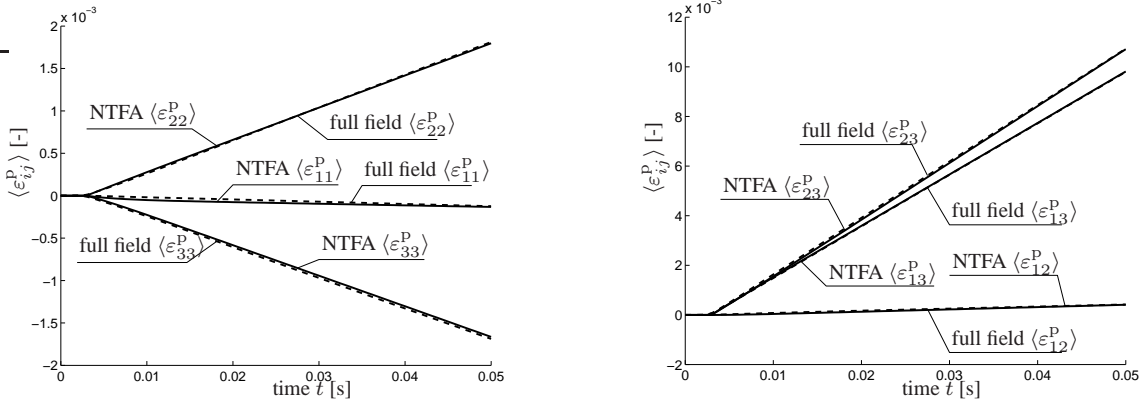


Figure 6: Time history of  $\langle \varepsilon_{11}^P \rangle$ ,  $\langle \varepsilon_{22}^P \rangle$ ,  $\langle \varepsilon_{33}^P \rangle$  (left) and  $\langle \varepsilon_{12}^P \rangle$ ,  $\langle \varepsilon_{13}^P \rangle$ ,  $\langle \varepsilon_{23}^P \rangle$  (right)

### 4.3 Full field reconstruction

In order to evaluate the degree of the local approximation the full fields of the stress, (total and plastic) strain and the displacement have been reconstructed for the last increment of the analysis. Attention is confined to the 23-component of the stress tensor.

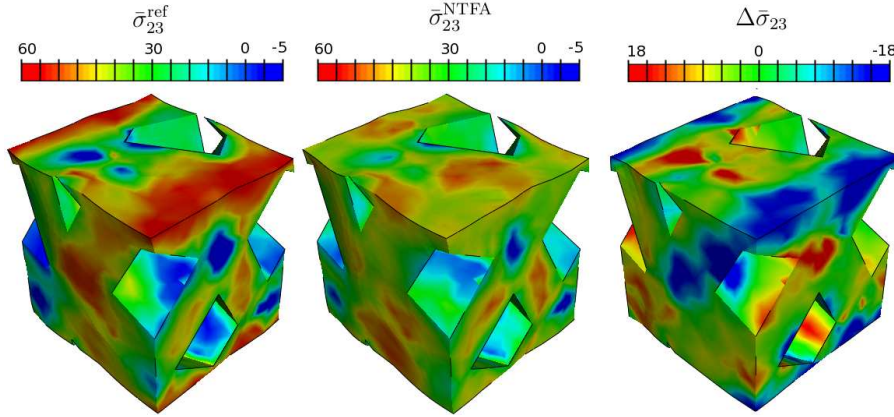


Figure 7: Magnitude of  $\sigma_{23}$  of the full field simulation (left), the NTFA reconstruction (middle) and the difference  $\sigma_{23}^{\text{NTFA}} - \sigma_{23}^{\text{ref}}$  (right) (metal matrix shown only)

Figure 7 shows the results of the full field simulation (left), the NTFA reconstruction (middle) and the difference between the two stress fields (right). We focus on the inelastic matrix material and, hence, have removed the elastic ceramic particles. By metric of vision the two fields show a good qualitative agreement. However, the reconstructed

stress field shows some deviations from the reference solution.

## 5. SUMMARY AND CONCLUSIONS

### 5.1 Summary

In section 2 we have briefly described a procedure for the generation of random three-dimensional model microstructures. The presented algorithm has the advantage that the particles have a constant distance to each other and arbitrarily high volume fractions are possible which is critical for many other algorithms. The main equations of the NTFA have briefly been revisited in Section 3. A comparison between a full field simulation at unit cell level and the results predicted by the NTFA is performed for a rather small number of only 6 inelastic modes. A good agreement has been found for the components of the macroscopic stress tensor. The agreement of the average plastic strain is excellent. Some quantitative deviations between the reconstructed stress field and the reference solution can be observed. However, the qualitative agreement is acceptable, i.e. stress concentrations are properly resolved.

### 5.2 Conclusions

The NTFA introduced by Michel and Suquet [11, 12] has been implemented for three-dimensional problems with random microstructures with a highly nontrivial geometry. Further investigations in this directions are subject of current investigations.

The results obtained from six inelastic modes and for the anisotropic microstructure examined are promising. The good agreement between reference computations found by Michel, Suquet and Roussette [11, 12, 13] for two-dimensional problems can be confirmed for three dimensions and more complex microstructures.

## References

- [1] S. Nemat-Nasser and M. Hori. *Micromechanics: Overall properties of heterogeneous materials*. Elsevier, 1999.
- [2] J.R. Willis. Bounds and self-consistent estimates for the overall properties of anisotropic composites. *Journal of the Mechanics and Physics of Solids*, 25:185–202, 1977.
- [3] T. Mori and K. Tanaka. Average Stress in a Matrix and Average Elastic Energy of Materials with Misfitting Inclusions. *Acta Metallurgica et Materialia*, 23:571–574, 1973.
- [4] E. Kröner. Berechnung der elastischen Konstanten der Vielkristalls aus den Konstanten des Einkristalls. *Z. Phys.*, 151:504–518, 1958.
- [5] F. Fritzen, T. Böhlke, and E. Schnack. Periodic three-dimensional mesh generation for crystalline aggregates based on voronoi tessellations. *Computational Mechanics*, 43(5):701, 2009. doi: 10.1007/s00466-008-0339-2.

- [6] C. Miehe. Strain-driven homogenization of inelastic microstructures and composites based on an incremental variational formulation. *Journal for Numerical Methods in Engineering*, 55:1285–1322, 2002.
- [7] F. Feyel. A multilevel finite element method (FE<sup>2</sup>) to describe the response of highly non-linear structures using generalized continua. *Computer Methods in Applied Mechanics and Engineering*, (192):3233–3244, 2003.
- [8] G.J. Dvorak and Y. Benveniste. On transformation strains and uniform fields in multiphase elastic media. *Proceedings of the Royal Society of London A*, (437): 291–310, 1992.
- [9] G.J. Dvorak, Y.A. Bahei-El-Din, and A.M. Wafa. The modeling of inelastic composite materials with the transformation field analysis. *Modelling and Simulation in Material Science and Engineering*, (2):571–586, 1994.
- [10] P. Suquet. *Continuum micromechanics*, volume 377 of *CISM Lecture Notes*, pages 197–264. Springer Verlag (New York), 1997.
- [11] J.C. Michel and P. Suquet. Nonuniform transformation field analysis. *International Journal of Solids and Structures*, (40):6937–6955, 2003.
- [12] J.C. Michel and P. Suquet. Computational analysis of nonlinear composite structures using the nonuniform transformation field analysis. *Computer Methods in Applied Mechanics and Engineering*, (193):5477–5502, 2004.
- [13] S. Roussette, J.C. Michel, and P. Suquet. Nonuniform transformation field analysis of elastic-viscoplastic composites. *Composite Science and Technology*, 69:22–27, 2009. doi: 10.1016/j.compscitech.2007.10.032.
- [14] F. Barbe, L. Decker, D. Jeulin, and G. Cailletaud. Intergranular and intragranular behavior of polycrystalline aggregates. Part 1: F.E. Model. *International Journal of Plasticity*, 17:513–536, 2001.
- [15] F. Aurenhammer. Voronoi Diagrams - A survey of a Fundamental Geometric Data Structure. *ACM Computing Surveys*, 23(3):345–405, 1991.
- [16] F. Feyel. *Application du calcul parallèle aux modèles à grand nombre de variables internes*. PhD thesis, Ecole National Supérieure des Mines de Paris, 1998.
- [17] J. Ohser and F. Mücklich. *Statistical Analysis of Microstructures in Materials Science*. Statistics in Practice. John Wiley & Sons, 2000.